

# Thermodynamics of a spin-1 Bose gas with fixed magnetization

Guillaume Lang and Emilia Witkowska

*Instytut Fizyki PAN, Aleja Lotników 32/46, 02-668 Warsaw, Poland*

(Received 26 June 2014; published 9 October 2014)

We investigate the thermodynamics of a spin-1 Bose gas with fixed magnetization including the quadratic Zeeman energy shift. Our calculations are based on the grand canonical description for the ideal gas and the classical field approximation for atoms with ferromagnetic and antiferromagnetic interactions. We confirm the occurrence of a double phase transition in the system that takes place due to two global constraints. We show analytically for the ideal gas how critical temperatures and condensed fractions are changed by a nonzero magnetic field. The interaction strongly affects the condensate scenario below the second critical temperature. The effect imposed by interaction energies becomes diminished in high magnetic fields where condensation of both ferromagnetic and antiferromagnetic atoms agrees with the ideal gas results.

DOI: [10.1103/PhysRevA.90.043609](https://doi.org/10.1103/PhysRevA.90.043609)

PACS number(s): 03.75.Mn, 05.30.-d, 05.70.Fh, 03.50.-z

## I. INTRODUCTION

A spinor Bose-Einstein condensate is a multicomponent condensate with an additional spin degree of freedom, which has provided exciting opportunities to study experimentally quantum magnetism, superfluidity, strong correlations, coherent spin-mixing dynamics, spin-nematic squeezing, entanglement, etc., most of them in nonequilibrium situations (see [1–6]). Despite successful experimental developments on spinor Bose-Einstein condensates, our knowledge remains limited regarding equilibrium properties and in particular the thermodynamics of such a gas. The main reason is the long time needed to reach an equilibrium state, typically several seconds or tens of seconds, which may exceed the lifetime of the condensate [7]. Nevertheless, recent experimental developments allowed for investigation of the ground state of an antiferromagnetic spinor condensate, providing the opportunity to study in detail its properties at thermal equilibrium [8].

The condensation of atoms with total spin  $F = 1$  trapped in the three hyperfine states  $m_F = 1, 0, -1$  in the absence of a magnetic field was investigated theoretically by Isoshima *et al.* [9]. The double-condensation phenomenon was predicted in the presence of two global conserved quantities: the total number of atoms  $N$  and the magnetization  $M$ . A condensate starts to appear in the highest  $m_F = 1$  component for temperatures below the first critical temperature and simultaneously in the two remaining components for temperatures below the second critical temperature. Analytical expressions for the two critical temperatures and condensate fractions were given for the ideal gas and zero magnetic field [9, 10]. The condensation of an interacting spin-1 Bose gas was considered numerically within the Bogoliubov-Popov approximation [9] and the Hartree-Fock-Popov approximation [11]. In the latter, authors confirmed the double phase transition for antiferromagnetic interactions, but found a more complicated phase diagram for ferromagnetic interactions with a possible triple-condensation scenario. The experimental work of Pasquiou *et al.* [12] touches upon the problem of the thermodynamics in chromium atoms with total spin  $F = 3$  but for free magnetization. Indeed, for low magnetic fields when the magnetization is approximately conserved the experimental results confirm the occurrence of a double condensation.

In this paper we reconsider the topic of condensation in the system of spin-1 bosons with fixed magnetization. The ultracold gases are almost perfectly isolated in the experiment and conservation of magnetization plays a major role. The magnetic dipole-dipole interactions, which may change the magnetization, are relatively weak and can be neglected for  $F = 1$  sodium or rubidium spinor Bose-Einstein condensates.

We examine the thermodynamics of the ideal gas in the presence of the quadratic Zeeman effect within the grand canonical ensemble. A nonzero magnetic field introduces a different phase in the phase diagram of critical temperatures that we characterize by the threshold magnetization. The condensation scenario predicted by Isoshima *et al.* is present for magnetizations larger than the threshold magnetization. When the magnetization of the system is smaller than the threshold magnetization, atoms start condensing not in the highest  $m_F = 1$  component, as was the case for the zero magnetic field, but in the  $m_F = 0$  component. That trivial effect is present due to the shift of the lowest energy level of the  $m_F = 0$  component below the lowest energy level of the  $m_F = 1$  component. We give an explicit expression for the threshold magnetization.

We study the interacting gas within the classical field approximation [13] combined with the Metropolis algorithm [14]. The method was successfully used to investigate thermal effects in the single-component Bose-Einstein condensates, including thermodynamics [15], vortex dynamics [16], a critical temperature shift [17], spin squeezing [18], solitons or the Kibble-Zurek mechanism [19], and many others, some of them reviewed in [20]. This numerical method includes all nonlinear terms present in the Hamiltonian at the expense of introducing a free parameter that has to be well chosen. In this paper we explain how to adapt the Metropolis algorithm for a spin-1 gas with fixed magnetization. To demonstrate the validity of the proposed algorithm we compare the results of simulations with exact results for the ideal gas and with the approximated Bogoliubov theory for antiferromagnetic interactions. We confirmed double condensation for both ferromagnetic and antiferromagnetic interactions. The condensation strongly differs from the result for an ideal gas below the second critical temperature. In the high-magnetic-field limit, when the quadratic Zeeman energy dominates over the

interaction energy, details of condensation do not depend on the interaction sign and are well described by the ideal gas results.

## II. MODEL

We consider a dilute and homogeneous spin-1 Bose gas in a magnetic field. We start with the Hamiltonian  $H = H_0 + H_A$ , where the symmetric (spin-independent) part is

$$H_0 = \sum_{j=-,0,+} \int d^3r \psi_j^\dagger \left( -\frac{\hbar^2}{2m} \nabla^2 + \frac{c_0}{2} n \right) \psi_j. \quad (1)$$

Here the subscripts  $j = -, 0, +$  denote sublevels with magnetic quantum numbers along the magnetic field axis  $m_F = -1, 0, +1$ ;  $m$  is the atomic mass; and  $n = \sum n_j = \sum \psi_j^\dagger \psi_j$  is the total atom density. The spin-dependent part can be written as

$$H_A = \int d^3r \left[ \sum_j E_j n_j + \frac{c_2}{2} : \mathbf{F}^2 : \right], \quad (2)$$

where  $E_j$  are Zeeman energy levels,  $\mathbf{F} = (\psi^\dagger f_x \psi, \psi^\dagger f_y \psi, \psi^\dagger f_z \psi)^T$  is the spin density,  $f_{x,y,z}$  are spin-1 matrices,  $\psi = (\psi_+, \psi_0, \psi_-)^T$ , and  $::$  denotes the normal order. The spin-independent and spin-dependent interaction coefficients are given by  $c_0 = 4\pi\hbar^2(a_0 + 2a_2)/3m$  and  $c_2 = 4\pi\hbar^2(a_2 - a_0)/3m$ , respectively, where  $a_s$  is the  $s$ -wave scattering length for colliding atoms with total spin  $S$ . The total number of atoms

$$N = \int n d^3r \quad (3)$$

and the magnetization

$$M = \int (n_+ - n_-) d^3r \quad (4)$$

are conserved quantities.

The linear part of the Zeeman shifts  $E_j$  induces a homogeneous rotation of the spin vector around the direction of the magnetic field. Since the Hamiltonian is invariant with respect to such spin rotations, we consider only the effect of the quadratic Zeeman shift.

For a sufficiently weak magnetic field we can approximate Zeeman energy levels by a positive energy shift of the  $m_F = \pm 1$  sublevels  $\delta = (E_+ + E_- - 2E_0)/2 \approx qh^2$ , where  $h$  is the magnetic-field strength and  $q = (g_I + g_J)^2 \mu_B^2 / 16E_{\text{hfs}}$ , with  $g_J$  and  $g_I$  the gyromagnetic ratios of the electron and the nucleus,  $\mu_B$  the Bohr magneton, and  $E_{\text{hfs}}$  the hyperfine energy splitting at zero magnetic field. Finally, the spin-dependent Hamiltonian (2) becomes

$$H_A = \int d^3r \left[ qh^2(n_+ + n_-) + \frac{c_2}{2} : \mathbf{F}^2 : \right], \quad (5)$$

where  $F_z^2 = n_+ - n_-$  and  $F_\perp^2 = 2|\psi_+ \psi_0^\dagger + \psi_0 \psi_-^\dagger|^2$  are the square of the magnetization density and the square of the transverse spin density, respectively. In spinor condensates realized in laboratories, the  $a_0$  and  $a_2$  scattering lengths have similar magnitude. The spin-dependent interaction coefficient

$c_2$  is therefore much smaller than its spin-independent counterpart  $c_0$ . For the  $^{23}\text{Na}$  condensate their ratio is about 1:30 and positive (antiferromagnetic order), while for the  $^{87}\text{Rb}$  condensate it is 1:220 and negative (ferromagnetic order).

By comparing the kinetic energy with the interaction energy, we can define the healing length  $\xi = 2\pi\hbar/\sqrt{2mc_0n}$  and the spin healing length  $\xi_s = 2\pi\hbar/\sqrt{2mc_2n}$ . These quantities give the length scales of spatial variations in the condensate profile induced by the spin-independent or spin-dependent interactions. Here we consider system sizes smaller than the spin healing length in order to avoid a domain formation. A good basis for such a homogeneous system is the plane-wave basis.

## III. IDEAL GAS

We consider a uniform gas of noninteracting atoms ( $c_0 = c_2 = 0$ ) with hyperfine spin  $F = 1$  in a homogeneous magnetic field  $h$  within the grand canonical ensemble, taking into account the quadratic Zeeman effect. The effective Hamiltonian of the system is

$$H_{\text{eff}} = \sum_{m_F=1,0,-1} \sum_{\mathbf{k}} (\epsilon_{\mathbf{k}} + m_F^2 q h^2) n_{\mathbf{k},m_F} - \mu N - \eta M, \quad (6)$$

with

$$N = N_+ + N_0 + N_- = \sum_{m_F} \sum_{\mathbf{k}} n_{\mathbf{k},m_F}, \quad (7)$$

$$M = N_+ - N_- = \sum_{m_F} \sum_{\mathbf{k}} m_F n_{\mathbf{k},m_F}. \quad (8)$$

Here  $\mathbf{k} = 2\pi/L(n_x, n_y, n_z)$ ,  $L$  is the system size,  $n_l = 0, \pm 1, \pm 2, \dots$  are integers, and  $n_{\mathbf{k},m_F}$  are occupation numbers of atoms of energy  $\epsilon_{\mathbf{k}} = \hbar^2 \mathbf{k}^2 / 2m$ . The chemical potential  $\mu$  and the linear Zeeman shift  $\eta$  are Lagrange multipliers enforcing the desired total atom number  $N$  and the magnetization  $M$ , respectively;  $N_{m_F}$  is the number of atoms in the  $m_F$ -th component. We consider a positive magnetization  $M \geq 0$  and a positive Zeeman energy shift  $qh^2 > 0$ .

The nonzero magnetic field removes the degeneracy of energy spectra

$$E_{\mathbf{k},+} = \epsilon_{\mathbf{k}} - \mu - \eta + qh^2, \quad (9)$$

$$E_{\mathbf{k},0} = \epsilon_{\mathbf{k}} - \mu, \quad (10)$$

$$E_{\mathbf{k},-} = \epsilon_{\mathbf{k}} - \mu + \eta + qh^2. \quad (11)$$

The ratio between  $\eta$  and  $qh^2$  determines the order of energy levels. The lowest energy level is  $E_+$  for  $qh^2 \leq \eta$  or  $E_0$  for  $qh^2 \geq \eta$ . In addition, two effects determine the state of the system: (i) the occupation number imbalance enforced by the fixed magnetization  $N_+ \geq N_-$  and (ii) the ground-state energy level ( $E_0$  or  $E_+$ ) controlled by the magnetic field.

Since the Hamiltonian is diagonal, we may calculate the grand canonical partition function

$$\Xi = \sum_{m_F, n_{\mathbf{k},m_F}} e^{-\beta E_{\mathbf{k},m_F} n_{\mathbf{k},m_F}}, \quad (12)$$

where  $\beta = 1/k_B T$ ,  $T$  is the temperature, and  $k_B$  is the Boltzmann constant. The ensemble average of the occupation

number  $n_{\mathbf{k},m_F}$  is

$$n_{\mathbf{k},m_F} = -\frac{1}{\beta} \frac{\partial \ln \Xi}{\partial E_{\mathbf{k},m_F}}, \quad (13)$$

which gives

$$n_{\mathbf{k},m_F} = \frac{z_{m_F} e^{-\beta \epsilon_{\mathbf{k}}}}{1 - z_{m_F} e^{-\beta \epsilon_{\mathbf{k}}}} \quad (14)$$

with effective fugacities

$$z_+ = e^{\beta(\mu + \eta - qh^2)}, \quad (15)$$

$$z_0 = e^{\beta\mu}, \quad (16)$$

$$z_- = e^{\beta(\mu - \eta - qh^2)}. \quad (17)$$

In the thermodynamic limit, keeping only dominant terms of  $O(N)$ , expressed in terms of fugacities, the number of atoms in the lowest energy level of each  $m_F$  component is

$$N_{m_F}^c = \frac{z_{m_F}}{1 - z_{m_F}}, \quad (18)$$

while the number of thermal atoms in each  $m_F$  component is

$$N_{m_F}^T = \left( \frac{L}{\lambda_{dB}} \right)^3 g_{3/2}(z_{m_F}), \quad (19)$$

where  $\lambda_{dB} = h/\sqrt{2\pi m k_B T}$  is the de Broglie wavelength and  $g_j(x) = \sum_{n=1}^{+\infty} x^n/n^j$  is the Bose function.

## A. Transition temperatures and condensate fractions

### 1. For $qh^2 \leq \eta$

*The first phase transition.* The first phase transition occurs for  $z_+ \rightarrow 1$  (or  $\mu \rightarrow qh^2 - \eta$ ) when the  $m_F = 1$  component starts condensing. That  $N_+^c \gg 1$  can be seen from (18). The number of thermal atoms is then

$$N_+^T = \left( \frac{L}{\lambda_{dB}} \right)^3 g_{3/2}(1), \quad (20)$$

$$N_0^T = \left( \frac{L}{\lambda_{dB}} \right)^3 g_{3/2}(e^{\beta qh^2} z_\eta), \quad (21)$$

$$N_-^T = \left( \frac{L}{\lambda_{dB}} \right)^3 g_{3/2}(z_\eta^2), \quad (22)$$

with  $z_\eta \equiv e^{-\beta\eta}$ . The first critical temperature  $T_{c1}$  can be obtained from the following equations:

$$N = \left( \frac{L}{\lambda_{dB}(T_{c1})} \right)^3 F_{3/2}^+(T_{c1}, z_{\eta c1}), \quad (23)$$

$$M = \left( \frac{L}{\lambda_{dB}(T_{c1})} \right)^3 [g_{3/2}(1) - g_{3/2}(z_{\eta c1}^2)], \quad (24)$$

where we have introduced the notation  $z_{\eta c1} \equiv z_\eta(T_{c1})$  and

$$F_{3/2}^+(T, z_\eta) \equiv g_{3/2}(1) + g_{3/2}(e^{\beta qh^2} z_\eta) + g_{3/2}(z_\eta^2). \quad (25)$$

Below  $T_{c1}$ , only the  $m_F = 1$  component condenses. It is justified to assume  $N_+^c \simeq N^c$ . Then relation  $N^c = N - \sum_\sigma N_\sigma^T$  defines the condensate fraction of the  $m_F = 1$  component

$$\frac{N_+^c}{N} \simeq 1 - \left( \frac{T}{T_{c1}} \right)^{3/2} \frac{F_{3/2}^+(T, z_\eta)}{F_{3/2}^+(T_{c1}, z_{\eta c1})}. \quad (26)$$

*The second phase transition.* The second phase transition occurs for  $z_\eta \rightarrow e^{-\beta qh^2}$  ( $\eta \rightarrow qh^2$ ) when  $N_0^c \gg 1$  and  $N_-^c \rightarrow e^{-2\beta qh^2}/(1 - e^{-2\beta qh^2})$ . In this regime  $T < T_{c2}$ , thermal populations are

$$N_+^T = \left( \frac{L}{\lambda_{dB}} \right)^3 g_{3/2}(1), \quad (27)$$

$$N_0^T = \left( \frac{L}{\lambda_{dB}} \right)^3 g_{3/2}(1), \quad (28)$$

$$N_-^T = \left( \frac{L}{\lambda_{dB}} \right)^3 g_{3/2}(e^{-2\beta qh^2}). \quad (29)$$

The second transition temperature  $T_{c2}$  can be obtained using the difference between the total atom number  $N$  and the magnetization  $M$ . For temperatures  $T \in [T_{c2}, T_{c1}]$ , in the absence of condensates in the  $m_F = 0, -1$  components, the difference is  $N - M \simeq 2N_-^T + N_0^T$ . The second transition temperature expressed in terms of Bose functions present in Eqs. (21) and (22) is

$$k_B T_{c2} = \frac{2\pi \hbar^2}{mL^2} \left[ \frac{N - M}{G_{3/2}(T_{c2})} \right]^{2/3}, \quad (30)$$

where

$$G_{3/2}(T) \equiv g_{3/2}(1) + 2g_{3/2}(e^{-2\beta qh^2}). \quad (31)$$

Below  $T_{c2}$ , the Bose-Einstein condensate can be formed in all components and condensate fractions satisfy the set of equations

$$N^c = M^c(T) + (N - M) \left[ 1 - \left( \frac{T}{T_{c2}} \right)^{3/2} \frac{G_{3/2}(T)}{G_{3/2}(T_{c2})} \right], \quad (32a)$$

$$N_+^c - N_-^c = M^c(T), \quad (32b)$$

$$\frac{2}{N_0^c} = \frac{1}{N_+^c} + \frac{e^{-2\beta qh^2}}{N_-^c} - 2 \sinh(\beta qh^2) e^{-\beta qh^2}. \quad (32c)$$

Here we have introduced the condensate part of the magnetization  $M^c \equiv M - M^T$  and the thermal part of magnetization

$$M^T(T) \equiv \left( \frac{L}{\lambda_{dB}} \right)^3 [g_{3/2}(1) - g_{3/2}(e^{-2\beta qh^2})]. \quad (33)$$

A derivation of Eqs. (32a)–(32c) is included in Appendix A. An analytical solution of Eqs. (32a)–(32c) is presented in Appendix B. We have checked the validity of the analytical solution against the self-consistent numerical result.

### 2. For $qh^2 \geq \eta$

First, one should note that this case does not exist in the absence of an external magnetic field since  $\eta$  can take positive values for  $M > 0$ . That is a new area of the phase diagram, which appears due to the quadratic Zeeman effect.

*The first phase transition.* This time, the  $m_F = 0$  component undergoes condensation first, which means that  $z_0 \rightarrow 1$  (or  $\mu \rightarrow 0$ ) and  $N_0^c \gg 1$ . One obtains new expressions for  $N_+^T$ ,

$N_0^T$ , and  $N_-^T$ , which hold under the critical temperature  $T_{c1}$ :

$$N_+^T = \left( \frac{L}{\lambda_{\text{dB}}} \right)^3 g_{3/2}(e^{-\beta q h^2} z_\eta^{-1}), \quad (34)$$

$$N_0^T = \left( \frac{L}{\lambda_{\text{dB}}} \right)^3 g_{3/2}(1), \quad (35)$$

$$N_-^T = \left( \frac{L}{\lambda_{\text{dB}}} \right)^3 g_{3/2}(e^{-\beta q h^2} z_\eta). \quad (36)$$

The first critical temperature  $T_{c1}$  and the fugacity at the critical point  $z_{\eta c1}$  can be obtained from the following equations:

$$N = \left( \frac{L}{\lambda_{\text{dB}}(T_{c1})} \right)^3 F_{3/2}^0(T_{c1}, z_{\eta c1}), \quad (37)$$

$$M = \left( \frac{L}{\lambda_{\text{dB}}(T_{c1})} \right)^3 \left[ g_{3/2}(z_{\eta c1}^{-1} e^{-q h^2 / k T_{c1}}) - g_{3/2}(z_{\eta c1} e^{-q h^2 / k T_{c1}}) \right], \quad (38)$$

where we have introduced

$$F_{3/2}^0(T, z_\eta) \equiv g_{3/2}(z_\eta^{-1} e^{-\beta q h^2}) + g_{3/2}(1) + g_{3/2}(z_\eta e^{-\beta q h^2}). \quad (39)$$

At the critical point the fugacity is smaller than one [ $z_\eta(T_{c1}) < 1$ ] since  $M \geq 0$  and  $g_{3/2}$  is an increasing function of its argument and takes positive values. Assuming that  $N_0^c \simeq N^c$  for  $T \in [T_{c2}, T_{c1}]$ , once again the relation  $N^c = N - \sum_{m_F} N_{m_F}^T$  defines the condensate fraction in the  $m_F = 0$  component

$$\frac{N_0^c}{N} \simeq 1 - \left( \frac{T}{T_{c1}} \right)^{3/2} \frac{F_{3/2}^0(T, z_\eta)}{F_{3/2}^0(T_{c1}, z_{\eta c1})}. \quad (40)$$

*The second phase transition.* One expects  $z_\eta \sim e^{-\beta q h^2}$ , implying that the  $m_F = 1$  component starts condensing:  $N_+^c \gg 1$  and again  $N_-^c \rightarrow e^{-2\beta q h^2} / (1 - e^{-2\beta q h^2})$ . Nevertheless, in this regime we should define  $T_{c2}$  in the other way. Neither  $N$  nor  $N - M$  can be used anymore since they involve

$N_+^c / N$ , which is now unknown in the intermediate region of temperatures. The only solution is to use the magnetization  $M$  and define  $T_{c2}$  as the temperature for which  $N_+^c \simeq N_-^c \ll N$ , that is,

$$k_B T_{c2} = \frac{2\pi \hbar^2}{m L^2} \left( \frac{M}{g_{3/2}(1) - g_{3/2}(e^{-2q h^2 / k T_{c2}})} \right)^{2/3}, \quad (41)$$

which is equivalent to  $M = M^T(T_{c2})$ . This choice is justified in the thermodynamic limit when  $N \gg e^{-2\beta q h^2} / (1 - e^{-2\beta q h^2})$  and mathematically within our equations for  $\beta q h^2 \gg 1$  and any  $N$ . Below  $T_{c2}$ , condensate fractions satisfy the set of equations

$$N^c = N - \left( \frac{L}{\lambda_{\text{dB}}} \right)^3 \left[ 2g_{3/2}(1) + g_{3/2}(e^{-2\beta q h^2}) \right], \quad (42a)$$

$$N_+^c - N_-^c = M^c(T), \quad (42b)$$

$$\frac{2}{N_0^c} = \frac{1}{N_+^c} + \frac{e^{-2\beta q h^2}}{N_-^c} - 2 \sinh(\beta q h^2) e^{-\beta q h^2}, \quad (42c)$$

where only Eq. (42a) is different from the set of equations (32a)–(32c).

## B. Phase diagram

The nonzero magnetic field changes dramatically the phase diagram of the critical temperatures, which is shown in Fig. 1. The phase diagram consists of four phases  $A$ ,  $B$ ,  $B'$ , and  $C$  separated by the two critical temperatures  $T_{c1}$  and  $T_{c2}$ . Depending on the value of the temperature, the system can be  $A$ , a nondegenerate thermal gas;  $B$ , a condensate in the  $m_F = 1$  component;  $B'$ , a condensate in the  $m_F = 0$  component and thermal atoms in other components; or  $C$ , a condensate in the  $m_F = 0$  and 1 and, in the  $m_F = -1$  component, a gas with a non-negligible fraction of atoms in the lowest energy level for  $\beta q h^2 \ll 1$  or with a negligible fraction of atoms in the lowest energy level for  $\beta q h^2 \gg 1$ .  $A$

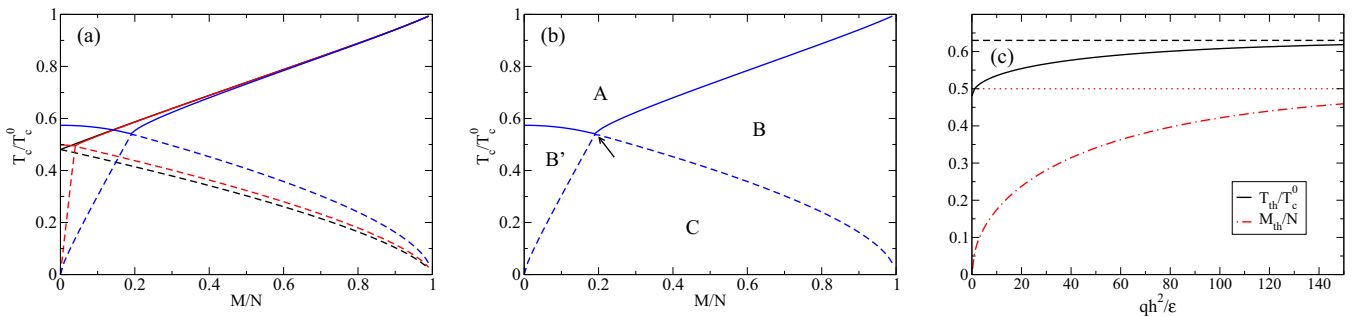


FIG. 1. (Color online) (a) and (b) Phase diagram of the critical temperatures, with  $T_{c1}$  marked by solid lines and  $T_{c2}$  marked by dashed lines. In (a) black lines are for  $qh^2 = 0$ , red lines are for  $qh^2 = 0.5\hbar^2/mL^2$ , and blue lines are for  $qh^2 = 12.5\hbar^2/mL^2$ . Here  $T_c^0 = (2\pi \hbar^2 / mL^2)[N/\zeta(3/2)]^{2/3}$  is the critical temperature for the one-component condensate in the box potential. (b) shows the same parameters for  $qh^2 = 12.5\hbar^2/2mL^2$ . The arrow indicates the threshold at the critical temperatures' intersection point. Particular parts of the diagram are  $A$ , thermal atoms (no condensate);  $B$ , condensate in the component  $m_F = 1$ ;  $B'$ , condensate in the component  $m_F = 0$  only; and  $C$ , condensate possible in all components. (c) Threshold temperature  $T_{\text{th}}/T_c^0$  (solid line) and the threshold magnetization  $M_{\text{th}}/N$  (dash-dotted line) at the critical temperatures' intersection point as a function of the quadratic Zeeman energy shift  $qh^2/\epsilon$  with  $\epsilon = \hbar^2/2mL^2$ . The asymptotic values of the threshold critical temperature  $T_{\text{th}}^\infty/T_{\text{th}}^0 = 2^{-2/3}$  and the threshold magnetization  $M_{\text{th}}^\infty = 1/2$  are marked by dashed and dotted lines, respectively. Here the total number of atoms is  $N = 10^4$ .

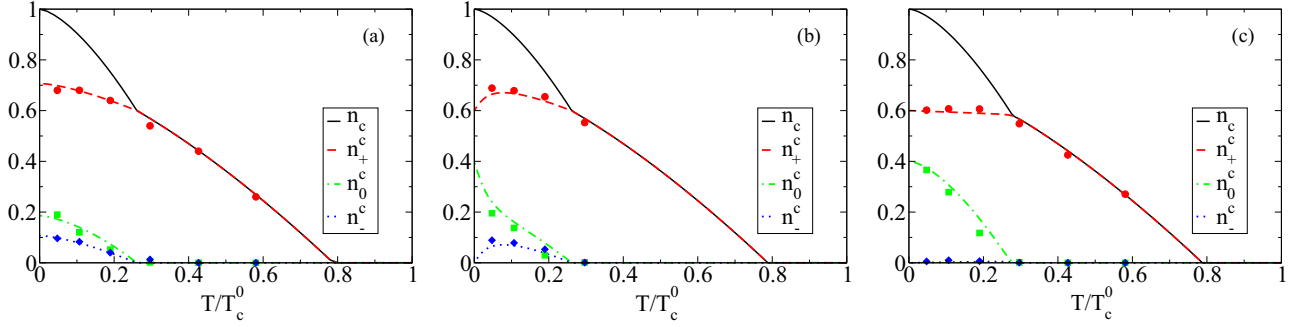


FIG. 2. (Color online) Condensate fractions for  $M > M_{\text{th}}$ , with  $N = 10^4$  and  $M = 6 \times 10^3$ , and (a)  $qh^2 = 0$ , (b)  $qh^2 = 0.1\hbar^2/mL^2$ , and (c)  $qh^2 = \hbar^2/mL^2$ . Here  $n_c = N^c/N$  is the total condensate fraction (solid black line),  $n_+^c$  is the condensate fraction in the  $m_F = 1$  component (dashed red line), and  $n_0^c$  and  $n_-^c$  are the condensate fractions in the  $m_F = 0$  (dot-dashed green line) and  $m_F = -1$  (dotted blue line) components, respectively. Lines are the solution of Eqs. (32a)–(32c), while points are the results of Monte Carlo simulations.

possible destination is controlled by the magnetization, with a special role for the threshold magnetization at the critical temperatures' intersection point  $M_{\text{th}} \equiv M(T = T_{c1} = T_{c2})$ . If  $M < M_{\text{th}}$  then to obtain particular quantities one should use expressions from Sec. III A 2 and in the opposite case ( $M > M_{\text{th}}$ ) from Sec. III A 1. The procedure to obtain numerical values for the critical temperatures is explained in Appendix C.

Analytical expressions for the threshold critical temperature  $T_{\text{th}}$  and the threshold magnetization  $M_{\text{th}}$  are

$$\left(\frac{T_{\text{th}}}{C}\right)^{3/2} = \frac{N}{2g_{3/2}(1) + g_{3/2}(e^{-2qh^2/k_B T_{\text{th}}})}, \quad (43)$$

$$\frac{M_{\text{th}}}{N} = \frac{3g_{3/2}(1)}{N} \left(\frac{T_{\text{th}}}{C}\right)^{3/2} - 1, \quad (44)$$

where  $C = \hbar^2/2\pi mL^2 k_B$ . The above expressions are obtained by comparing critical temperatures  $T_{c1}$  and  $T_{c2}$  for both  $qh^2 > \eta$  and  $qh^2 < \eta$ . In Fig. 1(c) we show the threshold critical temperature (43), the threshold magnetization (44), and their asymptotic values for  $\beta qh^2 \rightarrow \infty$ , which are  $T_{\text{th}}^\infty/T_{\text{th}}^0 \rightarrow 2^{-2/3}$  and  $M_{\text{th}}^\infty/N \rightarrow 1/2$ , respectively.

### C. Condensed fractions

Condensate fractions, i.e., solutions of Eqs. (32a)–(32c) for  $M > M_{\text{th}}$  and solutions of Eqs. (42a)–(42c) for  $M < M_{\text{th}}$ , are presented in Figs. 2 and 3, respectively, and are marked by lines. Points are the results of the Metropolis algorithm adapted to the model (more details concerning the algorithm can be found in Sec. IV B).

Figure 2 is for values of the magnetic field in the area  $M > M_{\text{th}}$  where  $qh^2 \leq \eta$ . These graphs show that modifications of condensed fractions occur mainly for low magnetic fields. The effect of the nonzero magnetic field is the most visible on the condensate fraction in the  $m_F = -1$  component. Notice that, at zero magnetic field, the fraction of the condensate in the  $m_F = -1$  component decreases simply with the temperature [see Fig. 2(a)]. In the transient magnetic-field regime, the condensed fraction in the  $m_F = -1$  component increases from zero, reaches a maximum, and then decreases to zero at the second critical temperature [see Fig. 2(b)]. The condensed fraction in the  $m_F = -1$  component decreases quickly and can be neglected in the high-magnetic-field regime [see Fig. 2(c)]. Condensate fractions are linked together when the condensed fraction of the  $m_F = -1$  component disappears, whereas the

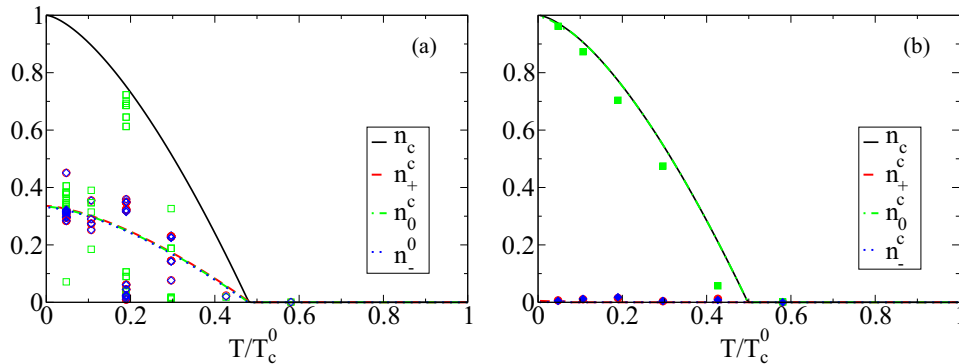


FIG. 3. (Color online) Condensate fractions for  $M < M_{\text{th}}$ , with  $N = 10^4$  and  $M = 50$ , and (a)  $qh^2 = 0$  and (b)  $qh^2 = \hbar^2/mL^2$ . Here  $n_c = N^c/N$  is the total condensate fraction (solid black line),  $n_+^c$  is the condensate fraction in the  $m_F = 1$  component (dashed red line), and  $n_0^c$  and  $n_-^c$  are the condensate fractions in the  $m_F = 0$  (dot-dashed green line) and  $m_F = -1$  (dotted blue line) components, respectively. Lines are the solution of Eqs. (42a)–(42c), while points are the results of Monte Carlo simulations. Particular points in (a) correspond to averaging over different representations of an ensemble and show strong fluctuations of condensate fractions in the regime of zero magnetic field and almost zero magnetization.

condensed fraction in the  $m_F = 1$  component decreases and the condensate fraction in the  $m_F = 0$  component increases. Nevertheless, the slope breaking that occurs at  $T_{c2}$ , already present when  $h = 0$ , is still neat. The fugacity varies dramatically near the zero temperature for small values of magnetic fields, which explains sharp variations of the condensed fractions in Fig. 2(b).

Figure 3 is for the magnetization  $M < M_{\text{th}}$  where  $qh^2 \geq \eta$ . The value of magnetization is  $M = 50$  and very small compared to  $N = 10^4$ ; therefore the difference between  $N_+^c$  and  $N_-^c$  is not visible. Notice the strong fluctuations of the condensate fractions for zero magnetic field that are results of Monte Carlo simulations [see the different points in Fig. 3(a)]. Indeed, for zero magnetization and zero magnetic field the ground state of the ideal gas is strongly degenerate [11], which gives rise to strong fluctuations of condensate fractions. The nonzero magnetic field reduces degeneracy and hence reduces fluctuations of condensate fractions in Fig. 3(b).

#### IV. INTERACTING GAS

The ground state of a spin-1 Bose gas in the presence of ferromagnetic and antiferromagnetic interactions was widely studied within the single-mode approximation [21] and beyond [22] and investigated in experiments for antiferromagnetic condensates [8]. The structure of the ground state is quite complex and depends not only on the magnetization and magnetic field but also on the relative phase between components of the Bose gas. It consists of a polar, nematic, or magnetic state and two-component or three-component solutions with phase and antiphase matching for ferromagnetic and antiferromagnetic interactions, respectively. We are aware of the temperature dependence of such structures, in particular the boundaries between different phases.

The nonzero temperature introduces a multimode structure, therefore we describe the system within the classical field approximation that takes into account thermal populations and interactions among many modes. Indeed, classical fields and stochastic methods [23] as well as Hartree-Fock or Hartree-Fock-Popov approximations [24] were applied for spinor condensates at nonzero temperature but for free magnetization. Among all of the finite-temperature methods that are used for single-component condensates, those like classical fields are not perturbative and thus contain all nonlinear terms that are present in the Hamiltonian. It makes them very suitable for studying thermodynamics in the whole temperature range, which is not the case for methods based on the Bogoliubov approximation. Below we just briefly recall the main concept of the classical field approach; more details concerning the foundations of the approximation can be found in [13].

##### A. Classical field approximation

The classical field approach consists of (i) replacement of the creation and annihilation operators by complex amplitudes and (ii) restriction of the summation over modes to a finite number extended all the way to the momentum cutoff  $\mathbf{K}_{\text{max}}$ . The field operator is replaced by a classical field (complex

function) of a well-defined number of momenta modes

$$\psi_j(\mathbf{r}) = \sum_{\mathbf{k} \leq \mathbf{K}_{\text{max}}} a_j(\mathbf{k}). \quad (45)$$

The energy  $E_\psi$  of such a classical field is given by discretization of the Hamiltonian  $H = H_0 + H_A$  [Eqs. (1) and (2)]. The total number of atoms is

$$N = \sum_j \sum_{\mathbf{k} \leq \mathbf{K}_{\text{max}}} |a_j(\mathbf{k})|^2 \quad (46)$$

and the magnetization is

$$M = \sum_{\mathbf{k} \leq \mathbf{K}_{\text{max}}} [|a_+(\mathbf{k})|^2 - |a_-(\mathbf{k})|^2]. \quad (47)$$

Various observables have a more or less pronounced dependence on the cutoff. Here we choose the cutoff momentum such that in the thermodynamic limit the noncondensed density for a single-component ideal Bose gas in the degenerate regime is exactly reproduced by the classical field model [25]. The condition gives  $E_{\mathbf{K}_{\text{max}}} \simeq 2.695k_B T$ , where  $E_{\mathbf{K}_{\text{max}}} = 3\hbar^2(\pi/L)^2/2m$  is the maximal kinetic energy on the grid.

##### B. Metropolis algorithm for a spin-1 Bose gas with fixed magnetization

We adapt the Metropolis scheme [14] to the system of classical fields as described in [15]. The main idea of this Monte Carlo method is to generate a Markovian process of a random walk in phase space. All states of the system visited during this walk become members of the statistical ensemble and are used in ensemble averages.

In order to obtain a statistical average of any observable  $A$ ,

$$\bar{A}_j = \frac{1}{\mathcal{N}} \sum_{s=1}^{\mathcal{N}} \langle \psi_j^{(s)} | A | \psi_j^{(s)} \rangle, \quad (48)$$

one should generate  $\mathcal{N}$  copies of the classical fields  $\psi_j^{(s)}$ . A canonical average is obtained in the limit  $\mathcal{N} \rightarrow \infty$  provided the number of members of the ensemble with energy  $E_\psi$  is proportional to the Boltzmann factor  $e^{-E_\psi/k_B T}$ . This can be achieved in a random walk where a single step of the Markov process is defined as follows.

(i) A set of amplitudes  $a_j^{(s)}(\mathbf{k})$  determines the state selected to be a member of the canonical ensemble at the  $s$ th step of the random walk. The corresponding energy  $E_\psi$  of the classical field is calculated according to (1) and (2). As the initial condition ( $s = 1$ ), any state that satisfies the condition of the fixed total number of atoms  $N$  and the magnetization  $M$  may be chosen as a member of the ensemble.

(ii) A trial set of amplitudes  $\tilde{a}_j^{(s)}(\mathbf{k})$  is generated by a random disturbance of  $\tilde{a}_j^{(s)}(\mathbf{k}) = a_j^{(s)}(\mathbf{k}) + \delta_j^{(s)}(\mathbf{k})$  followed by normalization to account for the total number of atoms. This way a trial classical field  $\tilde{\psi}_j^{(s)}$  is obtained. The corresponding magnetization  $\tilde{M}_s$ , energy  $\tilde{E}_{\tilde{\psi}_j}$ , energy difference  $\Delta_s = E_\psi - \tilde{E}_{\tilde{\psi}_j}$ , and the Boltzmann factor  $p_s = e^{-\Delta_s/k_B T}$  are then calculated.

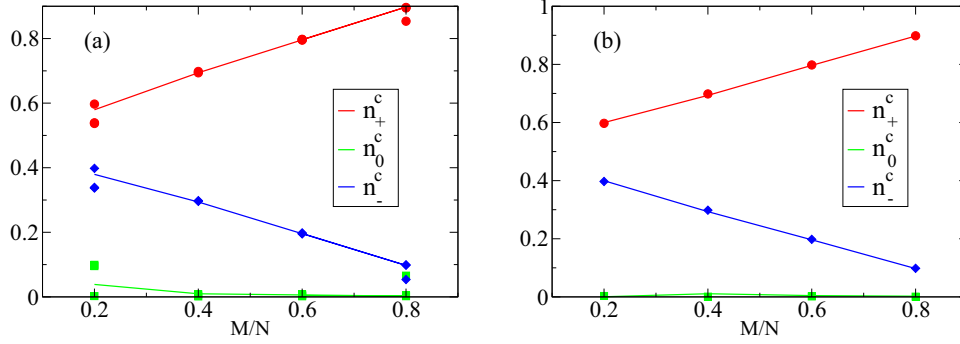


FIG. 4. (Color online) Test of the Metropolis algorithm for the  $^{23}\text{Na}$  spinor condensate in the low-temperature limit. The condensed fractions  $n_j^c$ , for  $j = \pm, 0$ , are plotted as a function of relative magnetization  $M/N$  for (a)  $qh^2 = 0$  and (b)  $qh^2 = 0.01\hbar^2/mL^2$ . Particular colors denote condensate fractions in the  $m_F = 1$  (red),  $m_F = 0$  (green), and  $m_F = -1$  (blue) components. Solid lines denote the Bogoliubov theory and points Monte Carlo results. The total number of atoms is  $N = 10^5$ .

(iii) If the magnetization  $\tilde{M}_s$  of a trial set of amplitudes satisfies  $|M - \tilde{M}_s| \leq \delta M$ , then  $\tilde{a}_j^{(s)}(\mathbf{k})$  can be considered as a new member of the ensemble.

(iv) A new member of the Markov chain  $a_j^{(s+1)}(\mathbf{k})$  is selected according to the following prescription: (a) If  $\Delta_s < 0$  then the trial state becomes a new member of the ensemble  $a_j^{(s+1)}(\mathbf{k}) = \tilde{a}_j^{(s)}(\mathbf{k})$  and (b) if  $\Delta_s > 0$  then a random number  $0 < u < 1$  is generated. If  $u < p_s$  then the trial state becomes a new member of the ensemble. In the opposite case  $u > p_s$ , the initial state  $a_j^{(s)}(\mathbf{k})$  is once more included in the ensemble  $a_j^{(s+1)}(\mathbf{k}) = a_j^{(s)}(\mathbf{k})$ .

The convergence of the procedure is the fastest when approximately every second trial state becomes a member of the ensemble. This factor depends on the assumed maximal value of displacements  $\delta_j^{(s)}(\mathbf{k})$  that can be modified during the walk. The parameter  $\delta M$  should be small enough to ensure almost constant magnetization  $M$ . Note that some number of initial members of the ensemble should be ignored in order to avoid the influence of the arbitrarily selected initial state of the system.

In order to demonstrate the validity of the algorithm we compare Monte Carlo simulations with the exact solutions for the ideal gas in Figs. 2 and 3 and with the approximated

Bogoliubov theory for the antiferromagnetic condensate in Fig. 4. In the latter case, analytical solutions are given by the Bogoliubov transformation for antiferromagnetic interactions and are valid in the low-temperature limit below the critical magnetic field [26]. Both comparisons are satisfactory, which allows us to use the algorithm in a wider range of interactions.

### C. Numerical results

In Figs. 5 and 6 we show the results of numerical simulations using the Metropolis algorithm. Figure 5 is for the magnetization  $M = N/2$  and Fig. 6 for  $M = 50$ . Condensate fractions for atoms with antiferromagnetic interactions are marked by closed points and those for atoms with ferromagnetic interactions by open ones. Particular colored symbols denote condensate fractions in the  $m_F = 1$  (red circles),  $m_F = 0$  (green squares), and  $m_F = -1$  (blue diamonds) components. Solid lines denote results for the ideal gas, added in the figures for comparison.

The double phase transition that occurs in the system as it is determined by the ideal gas calculations is clearly revealed. It does not seem that critical temperatures were affected very much by interactions. Moreover, even condensate fractions for the range of temperatures  $T \in [T_{c2}, T_{c1}]$  and any magnetic field follow the ideal gas prediction. It is not very

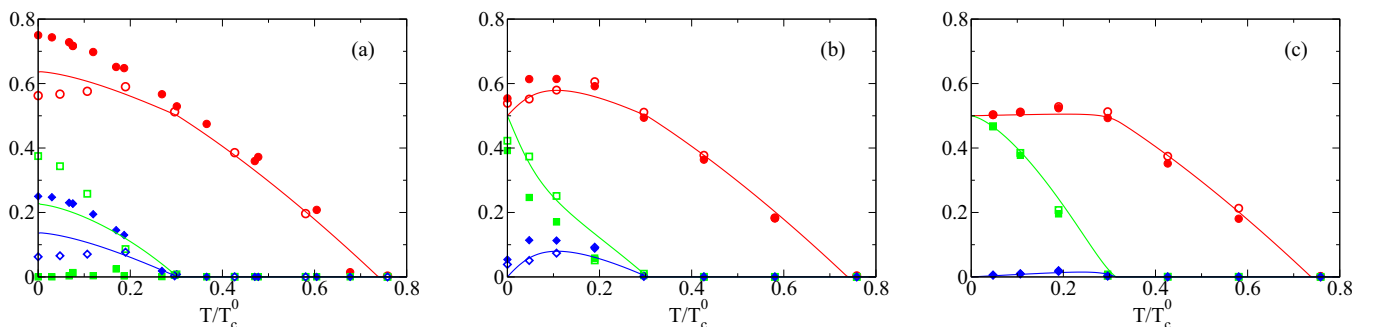


FIG. 5. (Color online) Condensate fractions for  $^{23}\text{Na}$  atoms with antiferromagnetic interactions (closed points) and  $^{87}\text{Rb}$  atoms with ferromagnetic interactions (open points). Particular colored symbols denote condensate fractions in the  $m_F = 1$  component (red circles),  $m_F = 0$  component (green squares), and  $m_F = -1$  component (blue diamonds). Solid lines are the results for the ideal gas. The total number of atoms is  $N = 10^4$ , the magnetization  $M = N/2$ , and the values of magnetic fields are (a)  $qh^2 = 0$ , (b)  $qh^2 = 0.124\hbar^2/mL^2$ , and (c)  $qh^2 = \hbar^2/mL^2$ .

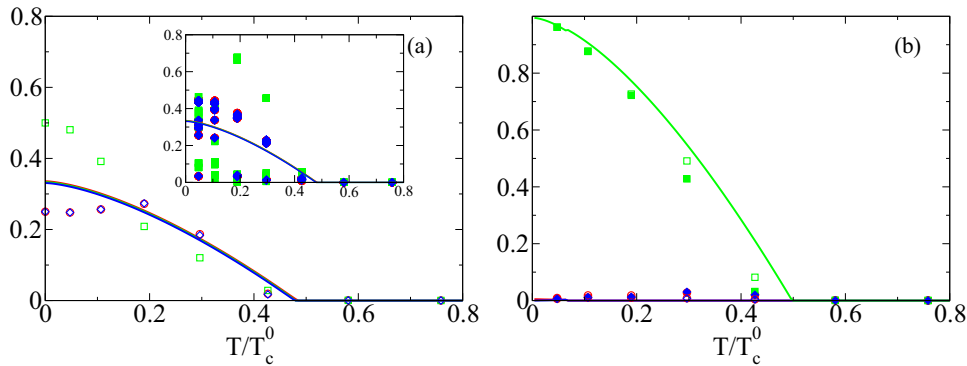


FIG. 6. (Color online) Same as in Fig. 5 but for magnetization  $M = 50$ . Condensate fractions for  $^{23}\text{Na}$  atoms with antiferromagnetic interactions are marked by closed points and for  $^{87}\text{Rb}$  atoms with ferromagnetic interactions by open points. Particular colored symbols denote condensate fractions in the  $m_F = 1$  component (red circles),  $m_F = 0$  component (green squares), and  $m_F = -1$  component (blue diamonds). Solid lines are the results for the ideal gas. The total number of atoms is  $N = 10^4$  and the values of magnetic fields are (a)  $qh^2 = 0$  and (b)  $qh^2 = \hbar^2/mL^2$ . In (a) condensed fractions for atoms with ferromagnetic interactions are presented in the main figure. Numerous points in the inset show condensate fractions for atoms with antiferromagnetic interactions that are obtained by averaging over different representations of ensemble members.

surprising since the system condenses in this regime like the single-component gas. Below the second critical temperature the condensate scenario results from the competition between spin-dependent interactions (dominant at low magnetic fields) and the quadratic Zeeman energy (dominant at large magnetic fields). The impact imposed by interactions is the most visible in the low-magnetic-field regime where ferromagnetic atoms condense differently than antiferromagnetic and neither matches the ideal gas curve [see Figs. 5(a) and 5(b)]. Nevertheless, dissimilarity in populations of a given component between both interaction types is not so large.

The antiferromagnetic interaction reduces the condensate population in the  $m_F = 0$  component in all of the temperature range for magnetic fields below its critical value known from the ground-state analysis [21] [see Fig. 5(a)]. Simultaneously, the condensate fraction in the  $m_F = \pm 1$  components decreases like  $(T/T_c^0)^{3/2}$ . The ferromagnetic interaction allows for condensation in all components and populations in the lowest momentum mode may decrease or increase up to the second critical temperature depending on  $m_F$ . In the other parameters regime condensate fractions may not simply decay with the temperature but may also increase up to some temperature, reach a maximum, and then decrease [see, e.g., the closed red points in Fig. 5(b)]. This feature is also observed for the ideal gas. In the high-magnetic-field regime, where the quadratic Zeeman energy dominates over the spin-dependent interaction energy, the condensate scenario matches the ideal gas prediction for both types of interactions, which can be seen in Figs. 5(c) and 6(b).

The interesting case of almost zero magnetization and zero magnetic field is presented in Fig. 6(a). We observe strong fluctuations of condensed fractions for atoms with antiferromagnetic interactions (shown in the inset), which is not the case for ferromagnetic atoms (shown in the main figure). In the inset of Fig. 6(a) numerous points are obtained by averaging over different representations of ensemble members. The results of the Monte Carlo simulations strongly fluctuate and additionally they are sensitive to the parameters of simulations (members of ensemble or  $\delta M$ , for example). Similar to the

ideal gas, the ground state of the antiferromagnetic condensate is degenerated, which gives rise to observed fluctuations. The phenomenon that is behind this effect is called spin fragmentation and has already been investigated theoretically for the antiferromagnetic spinor condensate [27].

## V. SUMMARY

We have studied the thermodynamics of a spin-1 Bose gas with fixed magnetization in the presence of a nonzero magnetic field. We have given explicit expressions for the two critical temperatures and all condensate fractions for the ideal gas. We have shown the occurrence of a peculiar phase in the phase diagram of critical temperatures. The interacting gas was studied within the classical field approach, which is not perturbative and includes all nonlinear terms present in the Hamiltonian. An alternative method, namely, the stochastic projected Gross-Pitaevskii equation, was recently adapted to the case of a spin-1 Bose gas but for free magnetization [23]. We found that interactions strongly affect the condensation scenario below the second critical temperature and for low magnetic fields. In this regime of parameters the thermodynamics of ferromagnetic and antiferromagnetic gases are different. The condensation is not affected much by interactions for values of temperatures between the two critical temperatures  $T \in [T_{c1}, T_{c2}]$  for all values of magnetic fields. Furthermore, the condensation is not affected by interactions in the whole temperatures range in the high-magnetic-field limit. Generalization to a Bose gas with arbitrary spin  $F$  is straightforward. Our results provide the opportunity to study the influence of a multimode structure on the properties of spinor condensates, providing an interesting direction for future work.

## ACKNOWLEDGMENTS

We thank M. Gajda and M. Matuszewski for useful discussions and O. Hul for a careful reading of the manuscript.

This work was supported by National Science Centre Grant No. DEC-2011/03/D/ST2/01938.

### APPENDIX A: EQUATIONS FOR CONDENSATE FRACTIONS WHEN $T \in [0, T_{c2}]$

Here we show how to obtain Eqs. (32a)–(32c) for condensed fractions. Equation (32a) is obtained by writing  $N_c = N_+^c + N_-^c + N_-^c = N - N^T$  in the form

$$N^c = N - \left(\frac{L}{\lambda_{\text{dB}}}\right)^3 [2g_{3/2}(1) + g_{3/2}(e^{-2\beta q h^2})]. \quad (\text{A1})$$

Then, after introducing  $G_{3/2}$  and  $M^T$ , it has the form

$$N^c = N - M^T(T) - \left(\frac{L}{\lambda_{\text{dB}}}\right)^3 G_{3/2}(T). \quad (\text{A2})$$

Knowing that  $N - M = (L/\lambda_{\text{dB}})^3 G_{3/2}(T)$ , after some algebra one finds Eq. (32a).

Equation (32b) is obtained just by rewriting the total magnetization in terms of its condensate and thermal parts  $M = (N_+^c - N_-^c) + (N_+^T - N_-^T)$  and an observation that the whole thermal part simply reduces to  $M^T(T)$ .

Equation (32c) is a bit more tedious to obtain. It is a peculiar case of a more general formula, valid in any regime, that we prove now. Starting from the set of equations

$$N_+^c = \frac{z_+}{1 - z_+}, \quad (\text{A3})$$

$$N_0^c = \frac{z_0}{1 - z_0} = \frac{z_+ z_\eta e^{\beta q h^2}}{1 - z_+ z_\eta e^{\beta q h^2}}, \quad (\text{A4})$$

$$N_-^c = \frac{z_-}{1 - z_-} = \frac{z_+ z_\eta^2}{1 - z_+ z_\eta^2}, \quad (\text{A5})$$

we rewrite

$$\frac{1}{N_+^c} = \frac{1}{z_+} - 1, \quad (\text{A6})$$

$$\frac{1}{N_0^c} = \frac{1}{z_+ z_\eta e^{\beta q h^2}} - 1, \quad (\text{A7})$$

$$\frac{1}{N_-^c} = \frac{1}{z_+ z_\eta^2} - 1, \quad (\text{A8})$$

which shows that

$$\frac{z_\eta e^{-\beta q h^2}}{N_-^c} + \frac{z_\eta^{-1} e^{-\beta q h^2}}{N_+^c} = \frac{2}{N_0^c} + 2 - z_\eta e^{-\beta q h^2} - z_\eta^{-1} e^{-\beta q h^2}, \quad (\text{A9})$$

which leads to Eq. (32c) in the limit  $z_\eta \rightarrow e^{-\beta q h^2}$ .

### APPENDIX B: ANALYTICAL SOLUTION OF EQUATIONS FOR CONDENSATE FRACTIONS WHEN $T \in [0, T_{c2}]$

Algebraic consideration of Eqs. (32a)–(32c) leads to the following equation for  $N_0^c$ :

$$N_0^{c3} + a N_0^{c2} + b N_0^c + c = 0, \quad (\text{B1})$$

where

$$a \equiv \frac{1 - 2u N_c + 2\tilde{u}}{u}, \quad (\text{B2})$$

$$b \equiv -\frac{2N_c \tilde{u} - 2M_{\text{eff}} u + 2N_c - u N_c^2 + u M_{\text{eff}}^2}{u}, \quad (\text{B3})$$

$$c \equiv \frac{N_c^2 - M_{\text{eff}}^2}{u}, \quad (\text{B4})$$

with  $u(q, h, T) \equiv \sinh(\beta q h^2) e^{-\beta q h^2}$  and  $\tilde{u}(q, h, T) \equiv \cosh(\beta q h^2) e^{-\beta q h^2}$ . The quadratic Zeeman effect transforms the equation for  $N_0^c$ , which is a second degree polynomial for the zero magnetic field, into a third degree polynomial. That polynomial has three roots. One needs to select, among those solutions, the only one that is physical: real, non-negative, and with values between 0 and  $N$ . To avoid numerical difficulties, one can find analytical solutions of this equation using, for instance, Cardan's method and select the one that has the proper limit when  $q h^2 \rightarrow 0$ . To do so we define

$$X \equiv N_0^c + \frac{a}{3}, \quad (\text{B5})$$

which allows us to put the polynomial into the form

$$X^3 + \tilde{p} X + \tilde{q} = 0, \quad (\text{B6})$$

with

$$\tilde{p} \equiv b - \frac{a^2}{3}, \quad (\text{B7})$$

$$\tilde{q} \equiv \frac{a}{27}(2a^2 - 9b) + c. \quad (\text{B8})$$

Then we write

$$X \equiv u + v \quad (\text{B9})$$

and note that  $u^3$  and  $v^3$  are solutions of

$$X^2 + \tilde{q} X - \tilde{p}^3/27 = 0. \quad (\text{B10})$$

Then we introduce

$$\Delta \equiv \frac{27\tilde{q}^2 + 4\tilde{p}^3}{27}. \quad (\text{B11})$$

Numerically, it appears that  $\Delta < 0$  and  $\tilde{p} < 0$ , which means that there are three solutions

$$X_k = 2\sqrt{-\tilde{p}/3} \cos \left[ \frac{1}{3} \arccos \left( -\frac{\tilde{q}}{2} \sqrt{\frac{27}{-\tilde{p}^3}} \right) + \frac{2k\pi}{3} \right], \quad (\text{B12})$$

where  $k \in \{0, 1, 2\}$ . To find  $N_{0k}^c$ , we have to keep in mind that

$$N_{0k}^c = X_k - \frac{a}{3}. \quad (\text{B13})$$

Eventually, we find that  $N_{01}^c$  should always be selected for  $N_0^c$  because it is the only solution that gives the appropriate limit when  $q h^2 \rightarrow 0$ . Then, having  $N_0^c$ , we can easily calculate  $N_+^c$  and  $N_-^c$  with Eqs. (32a) and (32b).

**APPENDIX C: HOW TO OBTAIN THE PHASE DIAGRAM**

In this appendix we explain how to compute numerically the transition temperatures  $T_{c1}$  and  $T_{c2}$  for any fixed magnetization. There is an additional difficulty in computing  $T_{c1}$  compared to the case when  $h = 0$  since its definition involves  $z_{\eta c1} \equiv z_{\eta}(T_{c1})$ , which is unknown. We can determine  $z_{\eta c1}$  from the constant of motion  $M/N$ , but to do so we have to know the value of  $T_{c1}$ , as can be seen from the following sets of equations:

$$T_{c1} \equiv C \left( \frac{N}{F_{3/2}^+(T_{c1}, z_{\eta c1})} \right)^{2/3}, \quad (C1)$$

$$\frac{M}{N} = \frac{g_{3/2}(1) - g_{3/2}(z_{\eta c1}^2)}{g_{3/2}(1) + g_{3/2}(e^{qh^2/k_B T_{c1}} z_{\eta c1}) + g_{3/2}(z_{\eta c1}^2)} \quad (C2)$$

if  $qh^2 \leq \eta$  and

$$T_{c1} \equiv C \left( \frac{N}{F_{3/2}^0(T_{c1}, z_{\eta c1})} \right)^{2/3}, \quad (C3)$$

$$\frac{M}{N} = \frac{g_{3/2}(e^{-qh^2/k_B T_{c1}} z_{\eta c1}^{-1}) - g_{3/2}(e^{-qh^2/k_B T_{c1}} z_{\eta c1})}{g_{3/2}(e^{-qh^2/k_B T_{c1}} z_{\eta c1}^{-1}) + g_{3/2}(1) + g_{3/2}(e^{-qh^2/k_B T_{c1}} z_{\eta c1})} \quad (C4)$$

if  $qh^2 \geq \eta$ . There are no further independent equations available for those two quantities, so they have to be solved in a self-consistent way.

Let us suppose that the magnetization is such that the system is in the area where  $qh^2 \leq \eta$ . We know the value of  $T_{c1}$  without a magnetic field and can sensibly expect that if a magnetic

field is switched on, the critical temperature will be of the same order of magnitude as it used to be, so we set the value of  $T_{c1}$  in the absence of any field  $qh^2 = 0$  to compute the value of  $z_{\eta c1}$  and then put this value into (C1) to compute the corrected value of  $T_{c1}$ , which can be used in (C2) to compute  $z_{\eta c1}$ . Those operations should be performed as many times as needed to make the effect of the wrong initial value disappear. The convergence is fast and after a few steps we are close to the fixed point for  $T_{c1}$ .

We can proceed in the same way using (C3) and (C4) if  $qh^2 \geq \eta$ , but how is it possible to know at once if we are in this case or in the other? We do not know it, but it is of no importance whatsoever if we use a little trick familiar to chemists. At the beginning we make some assumption and then check if the computed value  $z_{\eta c1}$  is consistent with this guess. If not, then it means that the assumption was wrong and that the system is in the other area. We should begin calculations again. Numerical problems can occur if we are really near the border between the two areas, so we need to be careful.

Eventually, to find the second critical temperature, we compute the only solution of the equation in  $T_{c2}$ ,

$$T_{c2} - C \left( \frac{N - M}{M^T(qh^2, T_{c2}) + 3g_{3/2}(e^{-2qh^2/k_B T_{c2}})} \right)^{2/3} = 0 \quad (C5)$$

if  $qh^2 \leq \eta$  or

$$T_{c2} - C \left( \frac{M}{g_{3/2}(1) - g_{3/2}(e^{-2qh^2/k_B T_{c2}})} \right)^{2/3} = 0 \quad (C6)$$

if  $qh^2 \geq \eta$ . The bisection method allows us to find this value with the requested accuracy, taking 0 for the lower bound and the temperature  $T_{c1}$  for the upper bound.

---

[1] D. M. Stamper-Kurn and M. Ueda, *Rev. Mod. Phys.* **85**, 1191 (2013).  
 [2] Y. Kawaguchi and M. Ueda, *Phys. Rep.* **520**, 253 (2012).  
 [3] Z. Zhang and L.-M. Duan, *Phys. Rev. Lett.* **111**, 180401 (2013).  
 [4] M.-S. Chang, Q. Qin, W. Zhang, L. You, and M. S. Chapman, *Nat. Phys.* **1**, 111 (2005); W. Zhang, D. L. Zhou, M.-S. Chang, M. S. Chapman, and L. You, *Phys. Rev. A* **72**, 013602 (2005); C. S. Gerving, T. M. Hoang, B. J. Land, M. Anquez, C. D. Hamley, and M. S. Chapman, *Nat. Commun.* **3**, 1169 (2012).  
 [5] T. M. Hoang, C. S. Gerving, B. J. Land, M. Anquez, C. D. Hamley, and M. S. Chapman, *Phys. Rev. Lett.* **111**, 090403 (2013).  
 [6] C. D. Hamley, C. S. Gerving, T. M. Hoang, E. M. Bookjans, and M. S. Chapman, *Nat. Phys.* **8**, 305 (2012).  
 [7] J. Guzman, G.-B. Jo, A. N. Wenz, K. W. Murch, C. K. Thomas, and D. M. Stamper-Kurn, *Phys. Rev. A* **84**, 063625 (2011).  
 [8] D. Jacob, L. Shao, V. Corre, T. Zibold, L. De Sarlo, E. Mimoun, J. Dalibard, and F. Gerbier, *Phys. Rev. A* **86**, 061601 (2012); J. Jiang, L. Zhao, M. Webb, and Y. Liu, *ibid.* **90**, 023610 (2014).  
 [9] T. Isoshima, T. Ohmi, and K. Machida, *J. Phys. Soc. Jpn.* **69**, 3864 (2000).  
 [10] Y. M. Kao and T. F. Jiang, *Eur. Phys. J. D* **40**, 263 (2006).  
 [11] W. Zhang, S. Yi, and L. You, *Phys. Rev. A* **70**, 043611 (2004).  
 [12] B. Pasquiou, G. Bismut, Q. Beauflis, A. Crubellier, E. Marechal, P. Pedri, L. Vernac, O. Gorceix, and B. Laburthe-Tolra, *Phys. Rev. A* **81**, 042716 (2010); B. Pasquiou, E. Marechal, L. Vernac, O. Gorceix, and B. Laburthe-Tolra, *Phys. Rev. Lett.* **108**, 045307 (2012).  
 [13] Y. Kagan and B. V. Svistunov, *Phys. Rev. Lett.* **79**, 3331 (1997); M. J. Davis, S. A. Morgan, and K. Burnett, *ibid.* **87**, 160402 (2001); A. Sinatra, C. Lobo, and Y. Castin, *ibid.* **87**, 210404 (2001); K. Góral, M. Gajda, and K. Rzążewski, *Opt. Express* **8**, 92 (2001); M. Brewczyk, P. Borowski, M. Gajda, and K. Rzążewski, *J. Phys. B* **37**, 2725 (2004).  
 [14] N. Metropolis *et al.*, *J. Chem. Phys.* **21**, 1087 (1953).  
 [15] E. Witkowska, M. Gajda, and K. Rzążewski, *Opt. Commun.* **283**, 671 (2010).  
 [16] C. Lobo, A. Sinatra, and Y. Castin, *Phys. Rev. Lett.* **92**, 020403 (2004); T. Karpiuk, M. Brewczyk, M. Gajda, and K. Rzążewski, *J. Phys. B* **42**, 095301 (2009); C. N. Weiler, T. W. Neely, D. R. Scherer, A. S. Bradley, M. J. Davis, and B. P. Anderson, *Nature London* **455**, 948 (2008).  
 [17] M. J. Davis and S. A. Morgan, *Phys. Rev. A* **68**, 053615 (2003).  
 [18] A. Sinatra, E. Witkowska, J.-C. Dornstetter, Y. Li, and Y. Castin, *Phys. Rev. Lett.* **107**, 060404 (2011); A. Sinatra, Y. Castin, and E. Witkowska, *Europhys. Lett.* **102**, 40001 (2013).

- [19] E. Witkowska, P. Deuar, M. Gajda, and K. Rzążewski, *Phys. Rev. Lett.* **106**, 135301 (2011); T. Karpiuk, P. Deuar, P. Bienias, E. Witkowska, K. Pawłowski, M. Gajda, K. Rzążewski, and M. Brewczyk, *ibid.* **109**, 205302 (2012).
- [20] *Finite Temperature and Non-Equilibrium Dynamics*, edited by S. Gardiner, N. Proukakis, M. Davis, and M. Szymanska (Imperial College Press, London, 2013), Vol. 1.
- [21] J. Stenger, S. Inouye, D. M. Stamper-Kurn, H.-J. Miesner, A. P. Chikkatur, and W. Ketterle, *Nature (London)* **396**, 345 (1998); W. X. Zhang, S. Yi, and L. You, *New J. Phys.* **5**, 77 (2003); K. Murata, H. Saito, and M. Ueda, *Phys. Rev. A* **75**, 013607 (2007); M. Matuszewski, T. J. Alexander, and Y. S. Kivshar, *ibid.* **80**, 023602 (2009).
- [22] M. Matuszewski, T. J. Alexander, and Y. S. Kivshar, *Phys. Rev. A* **78**, 023632 (2008).
- [23] A. S. Bradley and P. B. Blakie, *Phys. Rev. A* **90**, 023631 (2014).
- [24] N. T. Phuc, Y. Kawaguchi, and M. Ueda, *Phys. Rev. A* **84**, 043645 (2011); Y. Kawaguchi, N. T. Phuc, and P. B. Blakie, *ibid.* **85**, 053611 (2012).
- [25] E. Witkowska, M. Gajda, and K. Rzążewski, *Phys. Rev. A* **79**, 033631 (2009); A. Sinatra, E. Witkowska, and Y. Castin, *Eur. Phys. J. Spec. Top.* **203**, 87 (2012).
- [26] E. Witkowska, J. Dziarmaga, T. Świsłocki, and M. Matuszewski, *Phys. Rev. B* **88**, 054508 (2013).
- [27] L. DeSarlo, L. Shao, V. Corre, T. Zibold, D. Jacob, J. Dalibard, and F. Gerbier, *New J. Phys.* **15**, 113039 (2013).